Supercritical CO2 assisted extrusion foaming of PLA-cellulose fibre composites: effect of fibre on foam processing and morphology

Jennifer Andrea Villamil Jiménez, Salma Sabir, Martial Sauceau, Romain Sescousse, Fabienne Espitalier, Nicolas Le Moigne, Jean-Charles Bénézet, Jacques Fages

Supercritical CO_2 assisted extrusion foaming of PLA- cellulose fibre composites: effect of fibre on foam processing and morphology

Jennifer Andrea Villamil Jiménez[a b], Salma Sabir[a], Martial Sauceau [a], Romain Sescousse [a], Fabienne Espitalier [a], Nicolas Le Moigne [b], Jean-Charles Bénézet [b] and, Jacques Fages [a]

[a] Centre RAPSODEE, IMT Mines Albi, CNRS, Université de Toulouse, 81013 Albi, France;

[b] Polymers Composites and Hybrids (PCH), IMT Mines Alès, Université de Montpellier, 6 Avenue de Clavières, 30319 Alès, France

Abstract

This work is focused on the effect of the content and length of cellulose fibres on PLA foams produced by extrusion-foaming process assisted by sc-CO_2. The produced foamed samples were characterised by water pycnometry, modulated differential scanning calorimetry, and scanning electron microscopy. Increasing the length and the content of cellulose fibres results in a reduction of the expansion of the foams at a given die temperature. Nevertheless, long fibres at low content allows an increase of the longitudinal expansion of the foams. Furthermore, composite foams can be processed at a lower die temperature than neat PLA, providing a wider processing window. In general, the addition of cellulose fibres increases the crystallinity of the foams. Narrower cell size distributions and smaller cells are obtained when adding fibres, implying more homogeneous foam structures.

1 Introduction

The use of polymer foams in several fields of activity such as packaging, sound and heat insulation or filtration, ranging from the automotive industry for the realisation of dashboards or the padding of door panels, to the padding of children helmets or the packaging of refrigerated food products has raised the important problem of their environmental impact. A polymer foam or cellular polymer contains cavities filled with gas (cells) which allow to increase its flexibility, improve its insulating character, and make it damp or lighten it while keeping its structural properties [1]. In general, these foams are obtained from petroleum-based and non-biodegradable polymers such as polyurethane, polystyrene, polypropylene or polyethylene [2]. Due to the shortage of fossil resources and the rise of environmental issues and related societal concerns, biopolymers (biobased and/or biodegradable and/or biocompatible polymers) are more and more used [1].

Despite the general use of PLA in medical applications [3], its different properties have made PLA an appealing material for different industries [3–6], being one of the most studied biopolymers [7–9]. As it can be thought, the use of PLA as a polymer matrix for the production of foams has increased.

The manufacturing of foamy polymers requires the incorporation of blowing agents (chemical blowing agents CBAs and physical blowing agents PBAs). However, the use of these compounds poses several problems: in one hand, CBAs are generally carbonated salts that decompose into gas under the action of heat, leave residues in the polymer after the formation of the pore network and their decomposition often requires high temperatures. The use of these blowing agents for PLA has been already reported in the literature [10–13].

On the other hand, most PBAs, like freons, are harmful to the environment by attacking the ozone layer or like hydrocarbons such as pentane or butane pose safety concerns due to their flammability [14]. The technology of supercritical fluids, and more particularly supercritical CO_2 (sc-CO_2), could respond to these problems by offering an alternative free of the drawbacks just

mentioned. Indeed, CO_2 has the advantage of being non-toxic, non-polluting, non-flammable, and is neutral for the environment. It is available in high purity and at an affordable price. In the supercritical phase, it is soluble in large quantities in many polymers and therefore behaves as an excellent plasticiser [1].

Foaming with SFCs, though conceptually simple, is a complex dynamic process requiring full appreciation of the fundamentals of thermodynamics, physics, chemistry of solutions, interfaces, and interacting species; as well as polymer sciences and process engineering [15]. In general, the polymer is exposed to CO_2 at the operating pressure and temperature, which plasticises the polymer upon its solubilisation and reduces its apparent glass transition temperature and melting point [14]. During the depressurisation, the polymer becomes supersaturated in CO_2, and therefore nucleation of cells occurs. Then, the growth of the cells continues until the polymer solidifies [16]. The saturation pressure, the saturation temperature, and the depressurisation rate are the key parameters that determine the cell density and the cell size distribution in the final foam [16]. Different works report sc-CO_2 as a blowing agent being used with a wide range of polymers such as poly(methyl methacrylate) (PMMA) [17–19], polycarbonate [20–22], polyethylene terephthalate (PET) [23–25], polystyrene [26–29], glycol-modified PET [30,31], polyvinyl chloride (PVC) [32], polypropylene [33,34], polyurethane [35], polyimide [36], and polycaprolactone (PCL) [36–38]. Furthermore, the use of sc-CO_2 has extended to the foaming of (bio) composites [39–44], which shows the versatility of sc-CO_2 as a foaming agent.

The foaming of PLA using sc-CO_2 has been largely reported for the different foaming process, batch [45–54], semi-continuous (injection moulding) [55,56] and, continuous (extrusion) [53,57–60,60,61]. These works displayed that foaming of PLA is a challenge mainly due to its low melt strength and slow kinetics of crystallisation.

Melt strength can be described as the resistance of a molten polymer to stretching. It is a very important property during the foaming process, which, when low, can induce cell wall instability

through cell collapse and coalescence, leading to a heterogeneous foam morphology [62]. As for the crystalline phase, it could facilitate and induce bubble nucleation [63].

At present, a lot of methods have been proposed to enhance the foamability of PLA like chain branching [64–66], modifying the L/D ratio of PLA molecules [67,68], blending modification and crystallisation regulation [57,64,68–71]. The use of particles is considered as an option to limit the coalescence of cells, tailoring the melt strength of the polymer and its crystallisation [70–78]. Also, they contribute to the increase in the cell nucleation rate during foaming, acting as a heterogeneous nucleation agent [40–42,79].

Potential fillers can vary in origin from lignocellulosic fibres from different sources [80,81] to mineral ones, especially talc [72,73], clays [54], and silicates [82,83], as well as in terms of size, from micro [84] to nanoparticles [83,85,86], and shape. The presence of a filler in the polymer melt can increase the cell nucleation rate during foaming, acting as a heterogeneous nucleation agent [40–42]. Fillers can also increase the melt strength [72,73] and the crystallisation rate of PLA [74,75]. Compounding PLA with fillers does not only have foaming advantages but can also improve the performances of the final composites. When using lignocellulosic fibres, mechanical properties of the composite such as Young's modulus, tensile strength, elongation at break, among others, can be tailored by changing the characteristics and the amount of the fibre/filler [80].

The sc-CO_2 assisted extrusion process is widely described in the literature [1,87]. Recently this technology has been studied with biopolymers [1] because it allows to make "green" foams with a clean process. As the presence of a filler in the polymer melt does not only have foaming advantages, compounding a polymer with fillers can also improve the mechanical performances of the composites. The interest in foaming bio composites, especially PLA bio composites using sc-CO_2 assisted extrusion process has increased.

Thanks to the numerous researches carried out in the field of foaming PLA biocomposites with the sc-CO_2 assisted extrusion process [14], it has been shown that different morphologies and

properties can be obtained for the foams produced when a filler is added. However, the work in the literature mainly focuses on assessing the effect of the mere addition of different fillers or the operating conditions, without looking at how the properties of the fillers affect the morphological and functional properties of the produced foam. The fillers can be varied in terms of quantity, size, aspect ratio or even the chemical interactions they have with the polymer matrix. Cell morphology can be affected by each of these parameters. As a first approach to understanding the effects of these parameters, our work will focus on understanding the impact of varying the size and content of cellulose fibres on the morphology of PLA foams produced by extrusion foaming, which has not been comprehensively addressed in the available literature.

2 Materials and methods

2.1 Materials

An extrusion grade of polylactic acid (PLA) supplied by Natureplast France® was used as a polymer matrix for this work. Under the reference PLE 005A (amorphous) and in the form of translucent granules, this PLA has a melt flow index (MFI) of 3 g/10 min (210 °C; 2.16 kg), glass transition and melting temperatures of 61 °C and 157 °C respectively (obtained by Differential Scanning Calorimetry DSC), a Young's modulus of 3500 MPa (ASTM D882) and, a relative density of 1.25 (ASTM D792).

Cellulose fibres with different initial sizes were used and provided by J. Rettenmaier & Söhne Germany under the Arbocel® brand (BE60020: short fibres, BC200: long fibres). The fibres are mainly composed of cellulose, which represents 99.5 % of their composition. Shortened as S for short fibres and L long ones. Table 1 presents the characteristics of the fibres.

Table 1. Arbocel® fibres characteristics by J. Rettenmaier & Söhne Germany, determination of dimensions by air jet sieve analysis. Determination of bulk density by the method presented in DIN EN ISO 60.

Reference	Average fibre length	Average fibre width	Bulk density
	µm	µm	kg m^{-3}
Short (S)	23	17	240 - 300

Long (L)	300	20	35 - 55

2.2 Samples compounding

PLA was dried overnight at 50 °C under vacuum and, fibres were dried at 105 °C for two hours. A single-screw extruder CLEXTRAL BC21 900 mm was used to produce the composites, this extruder has a 900 mm long barrel (L) whose internal diameter (D) is 25 mm, which offers an L/D ratio of 36. The centre distance is 21 mm. The barrel is made up of nine modules of 100 mm each, which can be heated independently up to 250°C. In the first place, a masterbatch with 30 wt.% of fibres was obtained for both references (S and L). Then, to obtain composites with 5 wt.% and 15 wt.% of fibres (named respectively S_5, S_15, L_5 and L_15), the masterbatch was mixed with neat PLA and then extruded again. At the exit of the extruder, a cold-water bath was used to cool down the extrudate as well as a cold air flow right before a pelletiser. The obtained pellets were dried for 48 h at 50 °C.

2.3 Foaming

Fig. 1 corresponds to the extrusion system used for the foaming process, a Rheoscam SCAMEX extruder that has a single screw of 30 mm. This extruder has 4 zones. The first one has a length-diameter ratio (L/D) of 20 and the next two zones of 7.5, the three zones have a length of 1.05 m. The fourth part corresponds to a removable static mixer with an L/D of 2 (SMB H 17/4, Sulzer). A restrictor ring has been placed between the different zones of the extruder to prevent the upstream of the CO_2 injected into the barrel. The equipment temperature is measured and controlled in 6 heating zones distributed throughout it. Zones 1 and 2 are before the CO_2 injection, whilst 3 and 4 are after the injection, zone 5 is on the static mixer and, finally zone 6 is located in the die. Likewise, pressure is measured in 4 zones, zone 1 right after the injection zone, zone 2 after the gastight ring, zone 3 before the static mixer and, zone 4 right before the die. The dimensions of the extruder can be found in Table 2. The CO_2 is pumped up using a syringe pump 260D Isco by Serlabo. An annular die equipped with a pointed tip is used (Fig **2**), this die has a diameter of 6 mm and a length of 4 mm. It can be plugged by a tip with a tapered end. The pressure

exerted by this tip is adjusted by means of compressed air, which also makes it possible to adjust the pressure drop along the die and therefore the pressure of the polymer just before the die. Its primary function is to control and adjust the pressure P_4, in this case, at a value of 135 ± 5 bar.

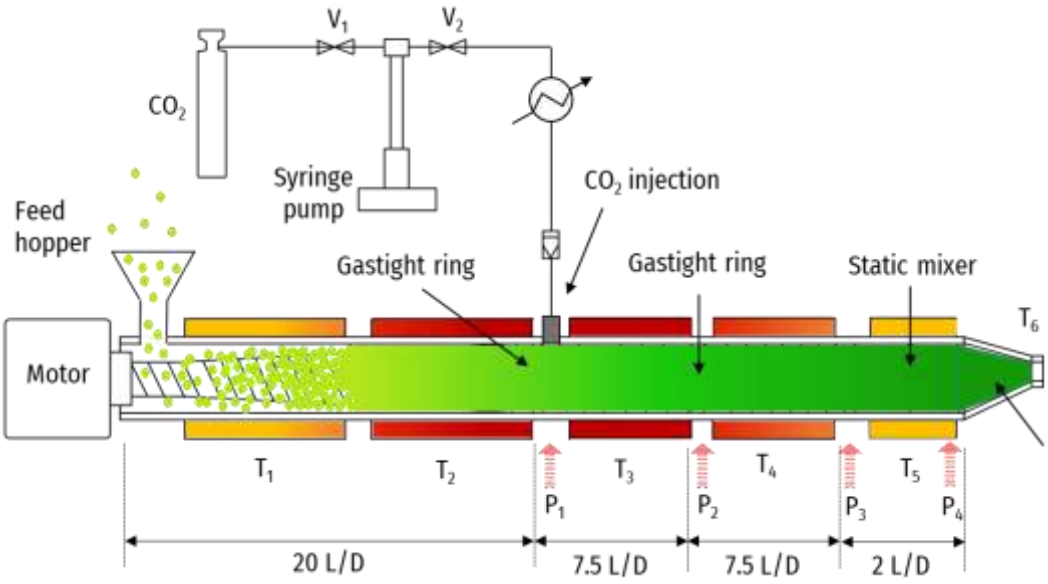

Fig. 1. Extrusion system with CO_2 injection.

Table 2. Dimensions of the extruder used for extrusion foaming process.

Length	1.05 m
Barrel diameter	30 mm
Screw body diameter	21 mm to 27 mm
Pitch	30 mm
Flight width	3.5mm
Channel depth	4.5 mm to 1.5 mm
Staggering angle	17.66°

Fig 2. Annular die.

The protocol has been already described in previous work [58,62]. Some operating conditions were kept constant, such as the screw speed N (30 rpm) and the temperature from T_1 to T_4 (T_1= T_2= T_3= 170 °C and T_4=160 °C), while T_5, T_6 (equal to T_5), and CO_2 volumetric flow rate (v_{CO2}) have been varied (2.5 mL min^{-1} and 3 mL min^{-1}). T_5 and T_6 were first set up at 160 °C without

CO_2 injection, then they were lowered together to get a high enough pressure inside the extruder to start the foaming experiments. At this moment, a constant CO_2 volumetric flow rate is injected and T_5 and T_6 were lowered together, and samples collected once the system has reached a steady state. The experiments were stopped when the syringe pump was empty, or the torque reached the safety limit of the apparatus.

The produced samples can be identified as X-T_6-v_{CO2}, where X corresponds to neat PLA or a composite (S_5, S_15, L_5 or L_15), T_6 corresponds to the die temperature (also known as foaming temperature) and, v_{CO2} the volumetric flow rate of CO_2 used to produce the sample (2.5 mL min^{-1} and 3 mL min^{-1}).

To determine the mass fraction of CO_2 (w_{CO2}) the following equation is used.

$$w_{CO2} = \frac{v_{CO2} * \rho_{CO2}^{PUMP}}{v_{CO2} * \rho_{CO2}^{PUMP} + \dot{m}_{POL}} \quad (1)$$

ρ_{CO2}^{PUMP} corresponds to the density of the CO_2 in the pump at 5 °C and at P_1 pressure in the injection point. This density was obtained via NIST (Span and Wagner equation of state). $\dot{m}_{POL}$ corresponds to the mass of a foamed sample taken during a certain time t at the exit of the extruder. All the data are available in the supplementary data section.

2.4 Foams characterisation

2.4.1 Porosity

The total porosity (ε_T), was calculated as follows:

$$\varepsilon_T = \frac{V_{POROSITY}}{V_{TOTAL}} = 1 - \frac{\rho_S^{H_2O}}{\rho_{POL}^{H_2O}} \quad (2)$$

Where: $\rho_S^{H_2O}$ is the sample density and $\rho_{POL}^{H_2O}$ represents the density of a non-foamed sample, both measured by water pycnometry (kg m^{-3}). A Borosilicate glass 3.3, DIN ISO 3507, Gay-Lussac type pycnometer was used.

The density of a sample i is determined by water pycnometry and calculated by using equation (3).

$$\rho_i^{H_2O} = \frac{m_i * \rho_{H_2O}}{m_{H_2O} + m_i - m_T} \quad (3)$$

Where:

ρ_{H_2O}: water density (taken as 1000 kg m^{-3}).

m_i: sample mass (kg).

m_{H_2O} : pycnometer full of water mass (kg).

m_T: pycnometer with water and sample i mass (kg).

2.4.2 Expansion

The total expansion is widely used in bibliography to express in a different scale the porosity of a foam. It was calculated as follows:

$$E_T = \frac{V_s}{V_{POL}} = \frac{\rho_{POL}^{H_2O}}{\rho_s^{H_2O}} = \frac{1}{1 - \varepsilon_T} \quad (4)$$

V_S is the volume of the foamed sample and V_{POL} is the volume of polymer in the same sample.

The maximum expansion (E_T^M) is calculated as follows (equation (5)). This is a theoretical value found under the assumption that all the solubilised CO_2 was used to foam the polymer (i.e. no CO_2 escape from the sample) [53]. The data for all samples are available in the supplementary data section.

$$E_T^M = 1 + \frac{w_{CO_2}}{1 - w_{CO_2}} * \frac{\rho_{POL}^{H_2O}}{\rho_{CO_2}^{AMBIENT}} \quad (5)$$

To find out the effectiveness of foaming, the expansion ratio (R_E) can be calculated as the ratio of expansion and the maximum expansion [53].

The radial expansion (E_R) is defined as the ratio of foamed sample diameter to non-foamed diameter ($D_{non\text{-}foamed} = 2.5$ mm), the diameter of the extrudate is measured using a calliper.

The longitudinal expansion (E_L) is also calculated by dividing the length of the foamed sample by that non-foamed at the same temperature and screw-rotation speed for the same time t ($L_{non\text{-}foamed}$ = 6.54 m during 1 min).

2.4.3 Thermal behaviour

A DSC Q200 by TA instruments was used with a constant dry nitrogen flow rate of 50 mL min^{-1} to ensure an inert atmosphere during the tests. An average temperature change of 2 °C min^{-1} with a sinusoidal amplitude of 0.8 °C and period of 40 s was used. The cooling rate was set at 10 °C min^{-1}. Depending upon the sample's given thermal history, a cold crystallisation exothermic peak may or may not be observed during the DSC experiment.

The initial degree of crystallinity only considers the crystallites formed during the processing of the foamed sample (i.e at the end of the foaming process) and it is calculated by using the equation (6).

$$\chi_o = \frac{\Delta h_m - \Delta h_{cc}}{\Delta h_m^\circ * (1 - x_{Fibres})} \quad (6)$$

The total degree of crystallinity corresponds to the crystallinity of the sample after the first heating scan in the DSC. It thus considers the crystallites formed during the foaming and the cold crystallisation phenomena upon heating in the DSC, and was calculated as follows:

$$\chi_c = \frac{\Delta h_m}{\Delta h_m^\circ * (1 - x_{Fibres})} \quad (7)$$

Where:

Δh_m: melting enthalpy of the sample (J g^{-1}).

Δh_{cc}: cold crystallisation enthalpy of the sample (J g^{-1}).

Δh_m° : melting enthalpy of a pure PLA crystal (taken as 93 J g^{-1}) [88].

x_{Fibres} : mass fraction of fibres within the sample (equal to 0 for neat PLA).

2.4.4 Cellular structure

To find the cell size and the cell density of foams, scanning electron microscopy (SEM) was used. Samples were fractured using liquid nitrogen to avoid as possible any damage of the morphology. The surface has been metallised (Metalliser SC7640 Polaron) with platinum under an argon atmosphere. A Thermoscientific Quattro S microscope by ThermoFisher scientific was used, the primary energy was 5 keV and a spot of 2 was used.

The average cell Feret diameter (D_c) and cell density are further determined from the SEM micrograph by using the software ImageJ. The average cell diameter corresponds to the D_{50} of the cell cumulated frequency distribution by number. The cell density (N_c) is calculated as follows:

$$N_c = \left[\frac{m}{A}\right]^{\frac{2}{3}} * \frac{\rho_{POL}^{H_2O}}{\rho_s^{H_2O}} \quad (8)$$

Where m is the number of cells on an SEM image, A is the area of the image.

Using 3 different samples produced under the same operating conditions (for 1 minute), the standard deviation σ of the different measurements of this work is calculated by using the equation (9).

$$\sigma = \sqrt{\frac{\sum_{i=1}^{n}(x_i - \bar{x})^2}{n-1}} \quad (9)$$

Where:

x_i: value of a measure.

$\bar{x}$: average of the population.

n: number of samples (n=3)

3 Results

3.1 Porosity

Fig. 3 shows the porosity of the produced foams. It is noticeable that the total porosity of composites is lower than that of neat PLA for each die temperature and volumetric flow rate of CO_2, this result has already been obtained by Bocz et al. [62] for PLA/cellulose and basalt foams. In general, the higher fibre content in the composite, the lower the porosity. The effect of the size is less evident, but it seems that the longer the fibre the lower the porosity. In addition, composites allowed to drop the die temperature more than the neat PLA, providing a wider processing window.

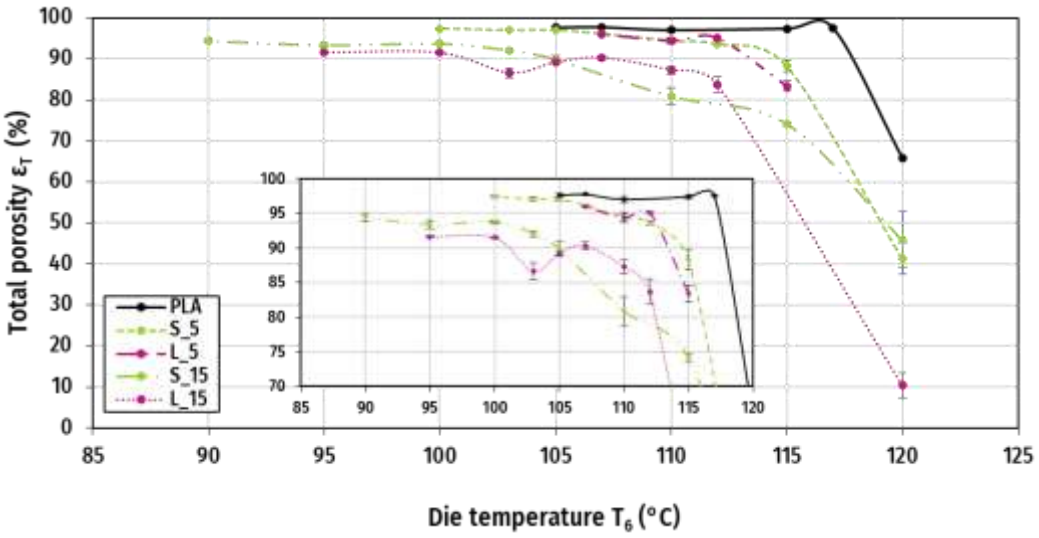

Fig. 3. Effect of die temperature on the total porosity of PLA-cellulose foams produced by sc-CO_2 assisted extrusion foaming. $v_{CO2} = 2.5$ mL min^{-1}. Continuous lines have been added to facilitate the visualisation of the graphs.

3.2 Expansion.

The results for the study of the expansion can be observed in Fig. 4. The longer the fibres the higher their content in the composite, the less the foam expands. In general, the expansion of the composites is more affected by the content of fibres than by their size. Regarding the expansion ratio, it was diminished when adding fibres. Composites with low fibre content and short fibres (S_5) achieved a higher radial expansion than net PLA at lower die temperature and higher sc-CO_2 flow rate (3 mL min^{-1}). It is also remarkable that the composite with longer fibres and low fibre content (L_5), produced high longitudinally expanded foams (Fig. 4.d) than neat PLA.

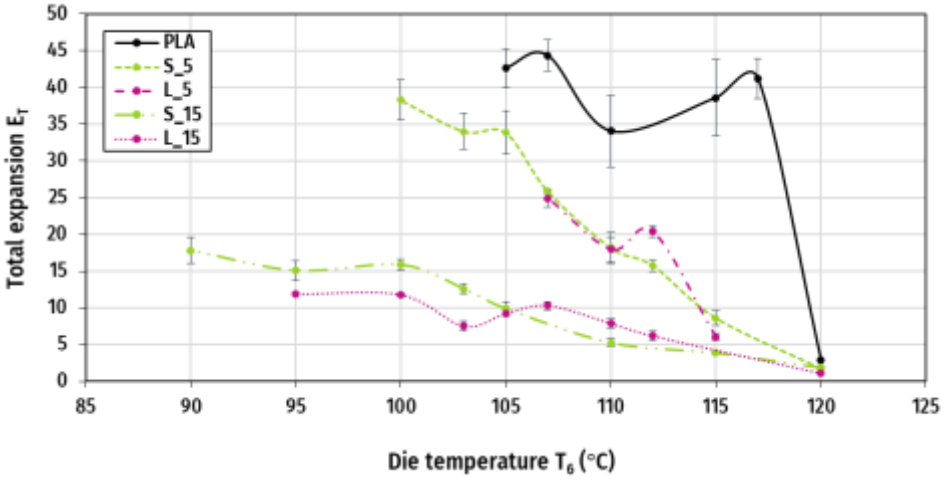
PLA
S_5
L_5
S_15
L_15
Total expansion E_T
Die temperature T_6 (°C)

a.

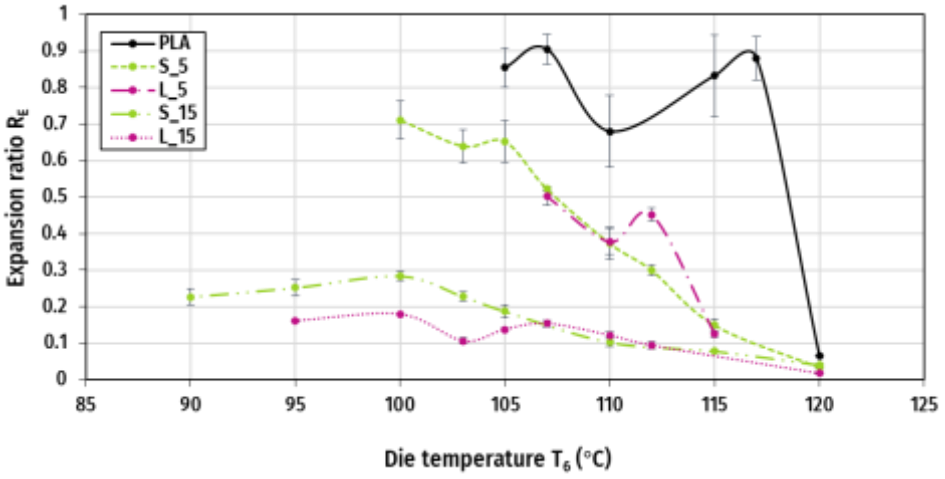
PLA
S_5
L_5
S_15
L_15
Expansion ratio R_E
Die temperature T_6 (°C)

b.

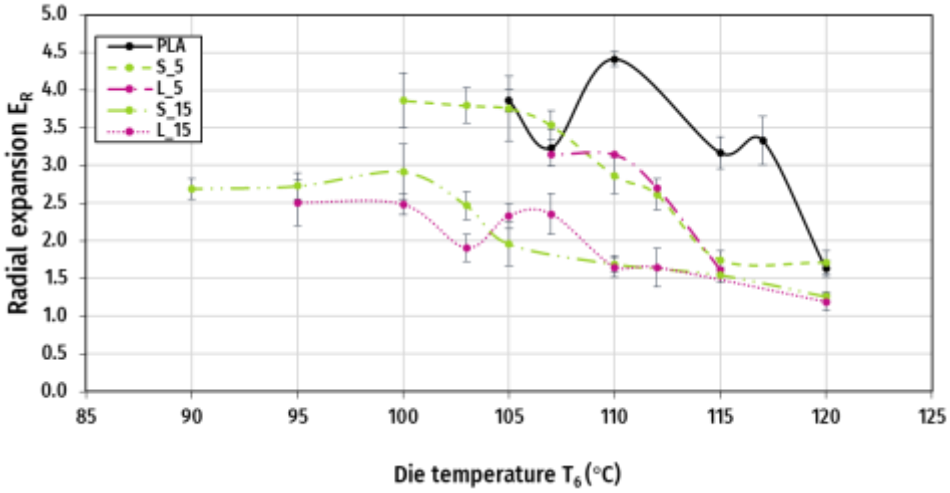
PLA
S_5
L_5
S_15
L_15
Radial expansion E_R
Die temperature T_6 (°C)

c.

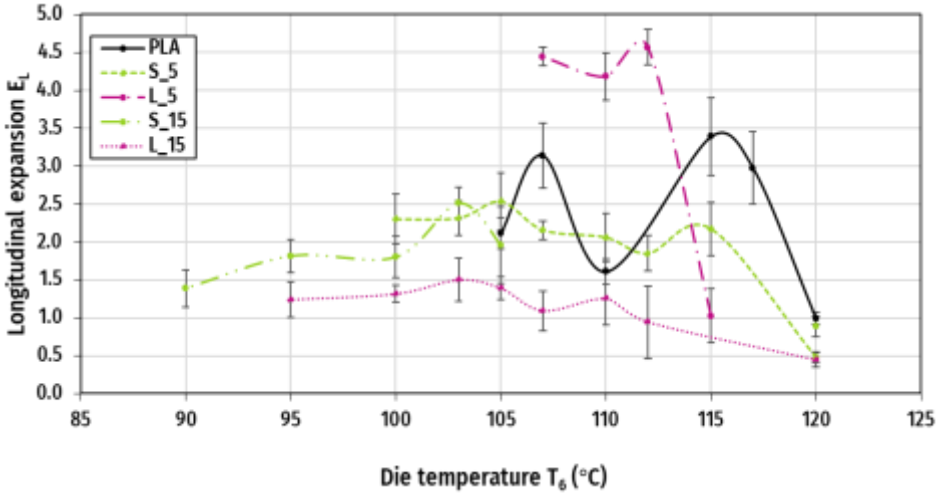

d.

Fig. 4. Effect of die temperature on **a.** total expansion, **b.** expansion ratio, **c.** radial expansion and **d.** longitudinal expansion of PLA-cellulose foams produced by sc-CO_2 assisted extrusion foaming. $v_{CO2} = 2.5$ mL min^{-1}. Continuous lines have been added to facilitate the visualisation of the graphs.

3.3 Thermal behaviour

Fig. 5 presents the thermograms of the foams produced at T_6= 120 °C and $v_{CO2} = 3$ mL min^{-1}. Table 3 presents the characteristic thermal parameters of PLA-cellulose foams produced by extrusion foaming determined by MDSC as well as the values for non-foamed extruded samples. These data correspond to the first heating run of the MDSC test. For all the analysed samples, the presence of a first endothermic event corresponding to the glass transition at around 59 to 60 °C is followed by an endothermic relaxation often attributed to secondary molecular rearrangement in the amorphous phase of the polymer [89]. Neither foaming with CO_2 nor the presence of fibres has any effect on the glass transition temperature of the samples.

All the samples presented a cold crystallisation peak which is commonly observed for PLA. At the same flow rate of CO_2, a decrease in the foaming temperature did not change the onset or the cold crystallisation peak temperatures. When increasing the volumetric flow rate of CO_2, the onset and peak temperatures slightly decreased. The onset and peak temperatures and the cold crystallisation enthalpy increased when adding the fibres, increasing their content, and increasing their size.

Regarding the melting process, an endothermic peak is observed for all the samples. All the melting peaks seem to start with a small "shoulder". No significant variations in melting peak temperature are noticed with changes in the die temperature or flow rate of CO_2. The onset melting temperature seems to slightly increase with the content and size of the fibres, while the melting peak temperature remains constant.

The initial crystallinity (χ_0) (crystallinity produced during the foaming process) of the foams is higher than that of the extruded PLA, which confirms the enhancing effect on crystallisation caused by sc-CO_2 reported in the literature [53,90,91] among others. Increasing the amount of sc-CO_2 increased the initial and the total (χ_c) crystallinity (after cold crystallisation). Decreasing the die temperature caused a slight increase in both crystallinities. Initial crystallinity increases with content and size of the fibres. Total crystallinity increases with content but remains unchanged when increasing the size.

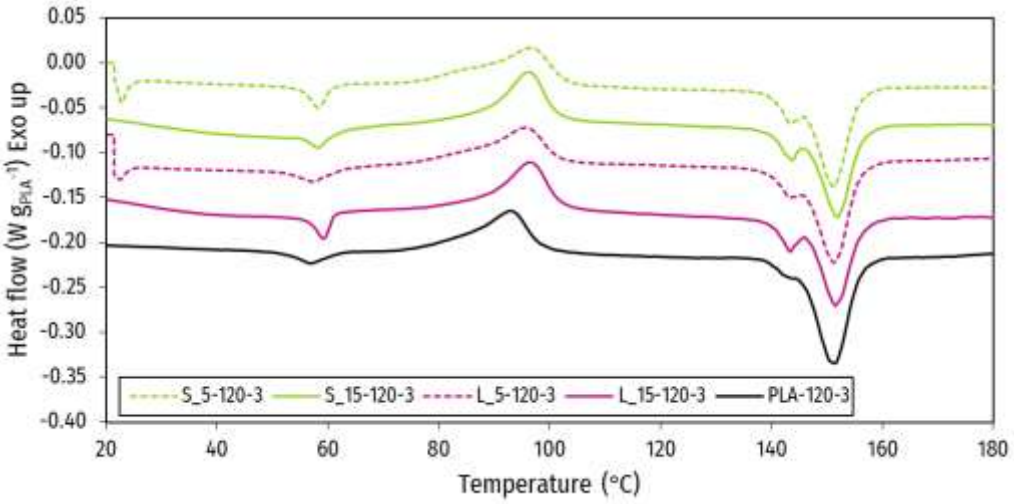

Fig. 5. MDSC 1st heating run of PLA-cellulose composite foams produced by extrusion foaming assisted by sc-CO_2. v_{CO2}= 3 mL min^{-1}. T_6 = 120 °C.

Table 3. Characteristic thermal parameters of PLA-cellulose foams produced by sc-CO_2 assisted extrusion foaming determined by MDSC.

Sample	Tg	T_{cc}		Δh_{cc}	T_m		Δh_m	χ_0	χ_c
		Onset	Peak		Onset	Peak			

	°C	°C		J g_{PLA}^{-1}	°C		J g_{PLA}^{-1}	%	%
					Non foamed				
PLA-170-0	59.1	89.5	97	21	139.6	144.4-152.2	22.8	1.9	24.6
S_5-170-0	59.5	89.6	96.2	22.2	139.5-146.7	143.7-151.9	27.0	5.1	29.0
S_15-170-0	59.5	90.7	93.4	30.6	140.15-146.7	143.2-152.4	33.1	2.8	35.6
L_5-170-0	59.1	90.4	97.3	22.0	143	146.8-152.4	29.1	7.6	31.2
L_15-170-0	59.8	87.4	94.3	27.7	145.6	152.6	33.9	6.7	36.5
					$v_{CO2} = 2.5$ mL min^{-1}				
PLA-105-2.5	59.2	80.9	93.1	17.9	143.9	150.9	26	8.7	28
PLA-107-2.5	59.2	79.8	92.9	16.8	143.9	150.6	25	8.8	26.9
PLA-110-2.5	60.2	80.6	92.9	15.9	144	150.4	23.3	8	25.1
PLA-120-2.5	60.3	86.8	93.8	20.4	143.4	151.7	26.7	6.8	28.7
S_5-100-2.5	59.1	75.3	86.1	12.2	141.4	150.4	27.8	16.8	29.9
S_5-105-2.5	59.9	75.5	94.5	11.8	143.9	150.2	24.8	14.0	26.7
S_15-90-2.5	58.7	70.0	91.5	10.0	141.7	149.9	31.9	23.5	34.3
S_15-105-2.5	60.0	82.9	94.7	18.3	143.6	150.5	32.3	15.1	34.8
S_15-110-2.5	59.8	82.9	94.9	18.3	143.7	151.2	31.5	14.3	33.9
L_5-107-2.5	59.0	74.3	93.0	16.5	144.0	150.9	25.5	9.7	27.4
L_5-112-2.5	60.2	76.4	91.2	14.6	143.8	150.5	25.8	12.0	27.7
L_15-95-2.5	59.0	79.3	93.4	13.7	143.1	150.3	34.0	21.8	36.6
L_15-105-2.5	59.9	73.8	94.1	16.3	142.7	150.3	33.2	18.1	35.7
L_15-112-2.5	59.8	77.5	95.1	21.9	143.7	150.8	31.9	10.7	34.3
					$v_{CO2} = 3$ mL min^{-1}				
PLA-100-3	59.0	76.4	90.6	11.3	141.4	149.9	28.2	18.2	30.4
PLA-105-3	60.0	76.2	91.3	12.1	142.1	150.8	28.2	17.3	30.4
PLA-110-3	59.1	75.5	90.5	14.4	142.5	150.2	29.5	16.2	37.1
PLA-120-3	59.3	82.0	93.0	18.3	144.7	151.4	27.0	9.4	29.1
S_5-100-3	59.3	73.9	90.2	12.6	141.4	150.4	27.8	16.3	29.9
S_5-105-3	60.2	75.0	94.2	12.0	142.4	150.5	25.8	14.9	27.7
S_5-112-3	59.9	74.3	92.4	11.8	141.8	150.0	26.2	15.5	28.2
S_5-120-3	59.6	84.2	96.5	19.4	145.0	151.2	26.5	7.6	28.5
S_15-103-3	59.8	73.5	94.5	14.5	143.3	150.2	31.1	17.7	33.4
S_15-110-3	60.1	82.7	94.9	15.0	143.5	150.7	23.5	9.2	25.3
S_15-120-3	59.5	88.0	96.1	23.8	145.5	151.8	31.8	8.6	34.2
L_5-105-3	59.8	74.0	85.6	10.2	143.9	150.0	28.0	19.1	30.2
L_5-110-3	58.8	73.2	94.1	16.8	144.5	150.8	24.4	8.2	26.3
L_5-112-3	60.4	77.9	95.7	15.6	144.6	150.9	23.4	8.4	25.2
L_5-120-3	59.6	84.3	95.5	17.5	144.8	151.2	27.5	10.7	29.5
L_15-105-3	59.2	70.3	94.4	15.5	144.1	150.4	32.2	17.9	34.6
L_15-112-3	60.1	80.9	95.3	17.3	143.9	150.2	31.2	15.0	33.6
L_15-120-3	59.9	88.0	96.6	23.7	145.6	151.4	31.5	8.4	33.8

3.4 Cell morphology

SEM microphotographs of fractured surfaces taken from the highly expanded foams are presented in Fig. 6. They are characterised by the presence of an inhomogeneous hollow and also retracted material, this is mainly caused by the type of die that is being used, since it has a moving

tip that allows the pressure to be regulated, which leaves its mark in the foam, modifying the structure. Besides, it can be observed that foams present a classic "honeycomb" structure. It is noticeable that long fibres at a high content did not allow to obtain a regular and homogeneous morphology. In the molten state, the high-loaded composites of long fibres (composites in the concentrated regime) tend to behave like a threshold fluid having a solid-like rheological behaviour. On cooling, it will solidify rapidly, so there will be no time for its expansion and the escaping gas will generate undefined and ragged cells. A skin of piled-up cells encircling the foam is observed for all of the samples, which seems to be thicker when increasing the size of the fibres. This skin is normally related to the cooling process of the sample at the exit of the die.

Scale= 5 mm* Scale = 2 mm Scale = 500 µm

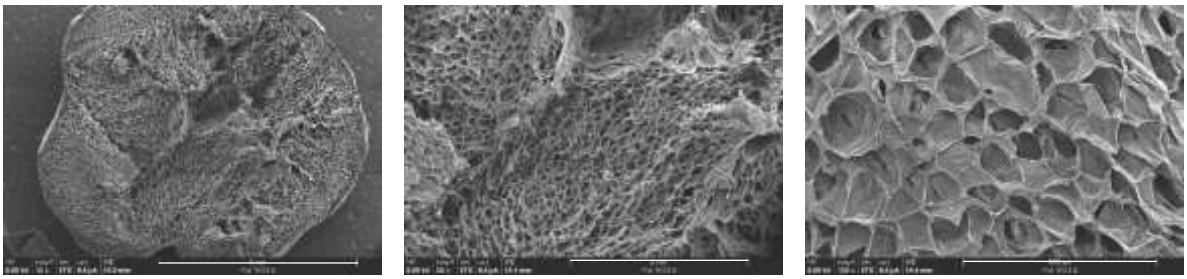

a. PLA-107-2.5

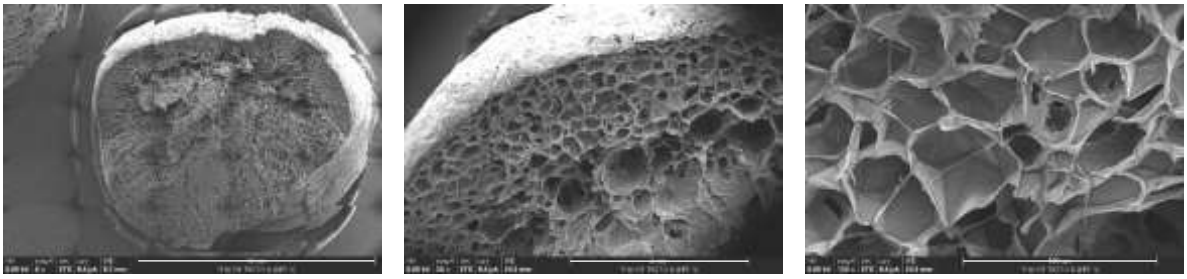

b. S_5-100_2.5

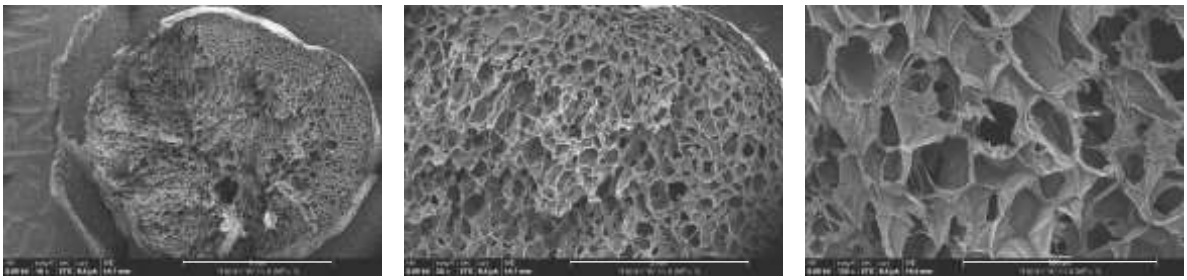

c. L_5-107-2.5

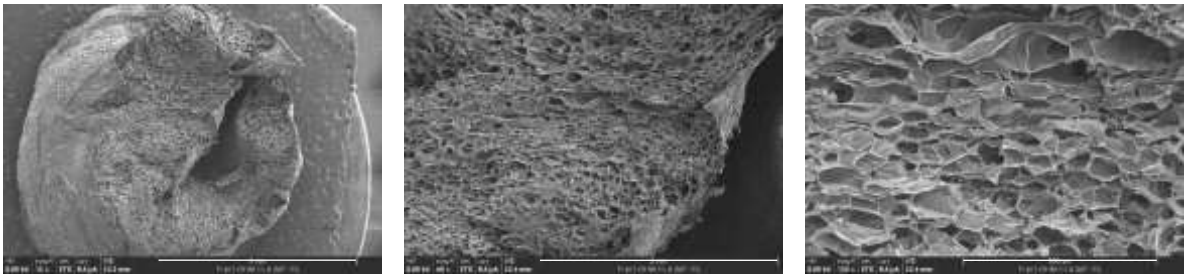

d. S_15-90-2.5

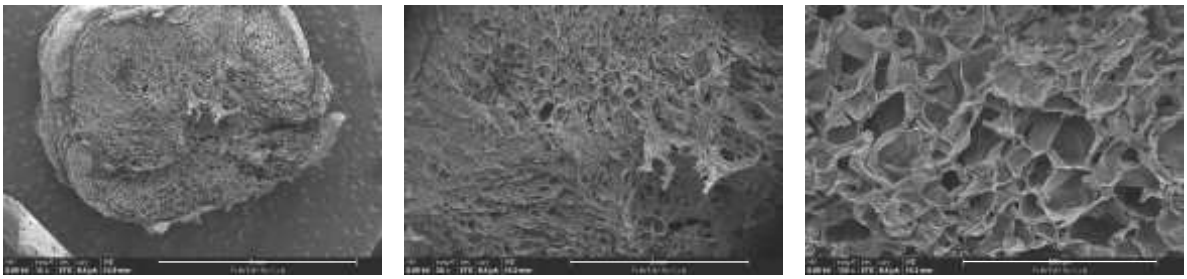

e. L_30-95-2.5

Fig. 6. SEM micrographs of PLA-cellulose highly expanded foams produced by sc-CO_2 assisted extrusion foaming. v_{CO2} = 2.5 mL min^{-1}.

* Scale of sample S_5-100-2.5 is 10 mm.

In Fig. 7, the cell size cumulated frequency distribution of the samples is shown, it can be observed that cell size was decreased when increasing the flow rate of sc-CO_2. When adding fibres, a decrease in the cell size can be observed as well. Narrower distributions are obtained when adding fibres, which implies more homogeneous structures. Increasing the content of fibres produced a more homogeneous structure with smaller cells than when increasing the size of the fibres. As already mentioned, a high content of long fibres did not produce a well-defined structure, which made these samples hard to analyse.

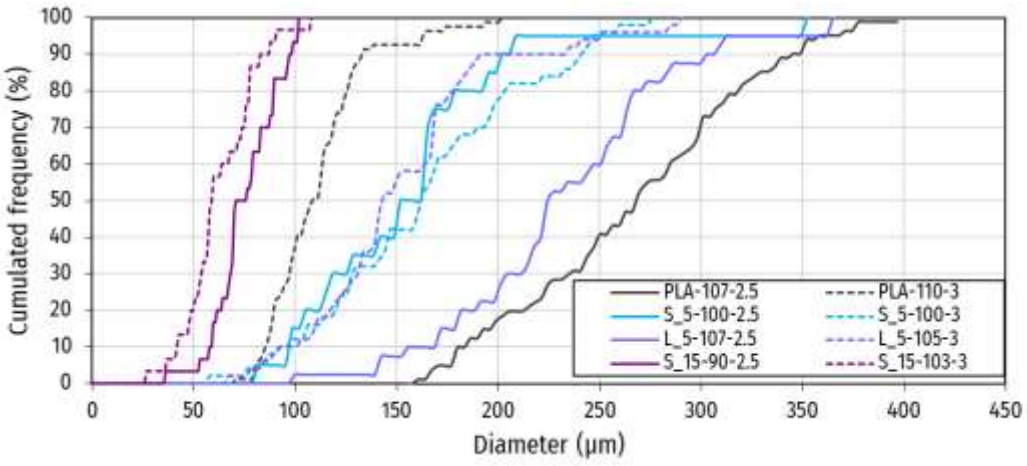

Fig. 7. Cell size cumulated frequency distribution of PLA-cellulose foams produced by sc-CO_2 assisted extrusion foaming process.

Table 4 provides data on the mean diameter and the cell density of the most expanded foams. It can be observed that in general the addition of fibres produced an increase in cell density and a decrease in cell size (diameter). In the same way, an increase in fibres content, produced an increase in cell density and a decrease in cell size. On the other hand, an increase in fibre length decreases the cell density and increases the cell size. In general, increasing the volumetric flow of sc-CO_2 produced foams with higher cell density and minor cell size.

Table 4. Morphological characteristics of the most expanded PLA-cellulose foams produced by sc-CO_2 assisted extrusion process.

Sample	D_c µm	N_c cells m^{-3}
PLA-107-2.5	269.2	$1.41x10^7$
S_5-100-2.5	153.5	$4.81 x10^7$
L_5-107-2.5	71.3	$6.32 x10^7$
S_15-90-2.5	225.7	$4.11 x10^7$
PLA-110-3	107.9	$1.38 x10^8$
S_5-100-3	164.2	$9.32 x10^7$
L_5-105-3	59.2	$1.51 x10^8$
S_15-103-3	145.9	$1.22 x10^8$

4 Discussion

The results will be discussed in two primary parts, the first corresponding to the effect of the die temperature on the PLA foams and, the second to the effect of the cellulose fibres.

4.1 Effect of the processing temperature

It was observed in the literature [58] that, the foaming temperature has a "threshold" value at which porosity decreases when decreasing temperature. When the temperature decreases, the diffusion of CO_2 in PLA decreases, thus gas escaping the from the polymer becomes more difficult [92]. In addition, the decrease in the temperature causes a solidification that will not allow the polymer to expand, so at a certain point, these two phenomena can provoke a decrease in the porosity which can be slightly seen at 100 °C in our range of temperature. On the other hand, when the temperature is high, the low viscosity allows a rapid movement of CO_2, which tends to escape quickly, without contributing to the foaming. Moreover, the cooling kinetics of the polymer at these temperatures does not allow the solidification of the matrix, the bubbles then collapse in on themselves decreasing total expansion.

As regards the study of expansion, longitudinal expansion increases as the CO_2 volumetric flow rate increases, while radial expansion decreases slightly as the flow rate increases. In both cases, longitudinal expansion is higher than radial. We know that the surface of the sample is exposed to the environment and therefore will cool and solidify faster than the inside. For the same die temperature, regardless of the CO_2 flow rate, this phenomenon occurs in the same way. However, in Table 3, it is observed that foams produced with 3 mL min^{-1} of CO_2 are more crystalline than those produced with 2.5 mL min^{-1}. It is well known that the crystallisation of a sample leads to its solidification. The foregoing allows us to conclude that foams produced at 3 mL min^{-1} of CO_2 were able to solidify slightly faster than those produced at 2.5 mL min^{-1} of CO_2 due to faster and improved crystallisation, preventing CO_2 from escaping and therefore generating less radial expansion.

Regarding the longitudinal expansion, as there is more CO_2 solubilised at 3 mL min^{-1} than at 2.5 mL min^{-1} and, the radial path is hindered by the solidification, consequently the gas passes through the inside of the extrudate in the flow direction, which is still hot and soft. This will create a more important longitudinal expansion than the radial one.

The results of the thermal behaviour showed that the glass transition temperature of PLA is not affected by the foaming process. The most remarkable result is that initial crystallinity increases when decreasing the foaming temperature and increasing the flow rate of sc-CO_2. The temperature is considered constant throughout the die and, according to Wang et al. [53], during the foaming process, most of the nucleation of crystals occurs at the die. It has been demonstrated that at moderated degrees of supercooling (from 100 to 110 °C), the crystallisation rate is at its maximum, and in general, the rates can be considered fast [93]. In addition, with the accelerating effect of sc-CO_2, higher crystallinities can be expected when reducing the die temperature.

Regarding the effect of the increasing amount of sc-CO_2, a higher content of dissolved gas promotes higher nucleation given the higher supersaturation of the polymer, Mihai et al. [90] showed that crystallinity was further developed by the biaxial stretching. So, if the stretching increases, crystallinity, increases as well. Finally, as it was shown by Jalali et al. [94] that, after applying pre-shear to a sample, it had a higher degree of crystallinity. This could indicate that a significant number of shear-induced nuclei had been formed, which mixed with the effect of sc-CO_2, can generate an increase in crystallinity.

A decrease in cell size and an increase in cell density were noticed when increasing the flow rate of sc-CO_2. From these results, we know that foams produced with a higher amount of sc-CO_2 present higher crystallinity, which is consistent with the enhancing effect of sc-CO_2 already explained in this work and in the literature. These crystals, likely generated in the die, can serve as nucleation sites for bubbles [90], consequently increasing the cell density and therefore, decreasing the cell size.

4.2 Effect of fibres

It was noticed that composites allowed to drop the die temperature more than the neat PLA, providing a wider processing window. After the compounding process, a noticeable decrease in viscosity was observed, reflecting a degradation of the polymeric matrix upon addition of the cellulose fibres. This, together with the plasticising effect of CO_2 may explain this result.

In general, the addition of fibres decreased the porosity and expansion of the PLA foams. It was noticed that, when increasing the amount of sc-CO_2, the reduction of the porosity caused by the fibres was more important. A reduction in porosity was measured by Le Moigne et al. [44] when foaming poly (3-hydroxybutyrate-co-3-hydroxyvalerate)/organo-clays composites. In this case, this result can be explained by the difference of the die pressure caused by the plasticizing effect of the gas in the polymer. As for these experiences, the die pressure remained constant, this behaviour is influenced by the enhanced crystallisation provided by the sc-CO_2. This is confirmed by the high crystallinity observed for the foams produced at 3 mL min^{-1} (see Table 3).

Regarding the study of the expansion, generally, and according to literature, the presence of fibres hinders the cells from expanding radially as well as the frozen skin at the outer surface of foams inhibit these cells and push the gas towards the longitudinal axis [58]. Thanks to SEM images, it was possible to observe that composites have a wider cooled skin with stacked cells than neat PLA. The thickness of this skin increases as the amount of added fibres also increases. In the results section, it was noticed that the composite with longer fibres and less charged (L_5), produced high longitudinally expanded foams compared to the rest of the samples. The work presented by Qian et al. [95] showed that when the total fibre volume ratio is increased even to 4%, the percentage of the fibre aligned along the extrusion direction is high. As long as the composite L_5 possesses a fibre volume ratio inferior to 4%, we can hypothesize that longer fibres oriented in the direction of the flow, served as guides for the exit of the gas, provoking a higher longitudinal expansion. Furthermore, given the limited interfacial adhesion between the fibres (which, for this work, were not functionalised) and the matrix, the local debonding could favour the pass of the gas. Cryofracture cutting of samples in the direction of flow, coupled with SEM observations, could help corroborate this hypothesis.

It was revealed during the MDSC tests, that the volumetric flow rate of sc-CO_2 was not important in the thermal properties of the composite foams produced. This result shows a different behaviour compared with neat PLA, where the flow rate of gas was important for the crystallinity of the samples. It can be suggested that, in the presence of fibres, the effect of the supercritical

CO_2 is less important. For the expansion ratio, it can be noticed that, for both flow rates, the behaviour and even the values are similar, indicating that the gas used for foaming was quite similar regardless to the initial flow rate. We can suggest that the fibres facilitated the escape of the gas from the polymer given the low interaction between the matrix and the fibres. So, the effect of fibres overlaps the effect of the gas producing foams with similar crystallinities.

In general, for the cellular morphology, foams with smaller and more uniform cell size distribution and larger cell density were obtained. Nevertheless, less uniform cells compared to the neat PLA were obtained. This can be linked to the fibre distribution within the polymer matrix and the interaction between these two components. In our case, no treatment was done for enhancing the interaction between PLA matrix and cellulose fibres. Many local matrix fibre debonding micro holes are induced, where the gas loss hinders the cell growth ability resulting in a non-uniform cell structure and limits gas expansion which decreases the porosity of foams [96].

5 Conclusions

PLA-Cellulose fibre composite foams were produced by supercritical CO_2-assisted extrusion. During the process the effect of temperature and volumetric flow rate of CO_2 on PLA and composite foams were studied. In general, as the die temperature decreased, the porosity and expansion increased until a maximum was reached at a temperature of 105 °C, and then decreased. When increasing the CO_2 volumetric flow rate, porosity, expansion (total, radial and longitudinal), cell size and crystallinity were increased. By adding fibres, generally the porosity, expansion (total and longitudinal) and cell size decreased, while radial expansion and degree of crystallinity increased. By adding fibres, in general the porosity, expansion (total and longitudinal) and cell size decreased, while radial expansion and degree of crystallinity increased. By increasing the fibre content in the matrix this trend is confirmed.

It can be remarked that the porosity of all samples is above 90 %, which means that high porosity foams can be obtained from the composite materials. Our result also reveals that it is possible to

master the cellular morphology of foam, not only by changing the processing conditions but also by mastering the length and content of cellulose fibres. Moreover, the addition of fibres widens the processing window in terms of temperature, which is an advantage for decreasing energy consumption and preserving material properties. Moreover, higher crystallinities were obtained when adding fibres. It is generally admitted in the literature that cellulose fibres should be functionalised to be more compatible with PLA and, consequently obtain higher porosities and more uniform foam morphologies. This work demonstrates that this is not necessarily needed to obtain such result.

Future research should delve into a comprehensive exploration of the effect of temperature profiles, screw speed, and die geometries on cell morphology. Understanding how these parameters influence the foaming process can provide valuable insights. Furthermore, an intriguing avenue for future investigation lies in simultaneously incorporating fibres and PLA at the same time during the foaming process (i.e. compounding and foaming at the same time). This approach has the potential to simplify the generation of biocomposite foams, offering a promising direction for advancing the efficiency and versatility of the manufacturing process.

The study of the mechanical, rheological, thermal, degradation and other properties of the foams produced can shed light on the different applications and future developments of these materials,

Acknowledgements

This research was funded by Région Occitanie in form of a doctoral scholarship to the first author.

References

[1] M. Chauvet, M. Sauceau, J. Fages, Extrusion assisted by supercritical CO_2: A review on its application to biopolymers, J. Supercrit. Fluids. 120 (2017) 408–420. https://doi.org/10.1016/j.supflu.2016.05.043.
[2] M. Biron, Polymères alvéolaires - Présentation et propriétés, Tech. Ing. (2003) 23.
[3] J.R. Lasprilla, A.R. Martinez, B.H. Lunelli, A.L. Jardini, R.M. Filho, Poly-lactic acid synthesis for application in biomedical devices: A review, Biotechnol. Adv. 30 (2012) 321–328. https://doi.org/10.1016/j.biotechadv.2011.06.019.

[4] R. Auras, B. Harte, S. Selke, An Overview of polylactides as packaging materials, Macromol. Biosci. 4 (2004) 835–864. https://doi.org/10.1002/mabi.200400043.
[5] De. Notta-Cuvier, A. Bouzouita, J. Odent, R. Delille, M. Murariu, F. Lauro, J.-M. Raquez, G. Haugou, P. Dubois, L'acide polylactique (PLA) pour des applications automobiles, Thecniques Ing. (2018) 19.
[6] J. Ahmed, S.K. Varshney, Polylactides—chemistry, properties and green packaging technology: A review, Int. J. Food Prop. 14 (2011) 37–58. https://doi.org/10.1080/10942910903125284.
[7] S. Farah, D.G. Anderson, R. Langer, Physical and mechanical properties of PLA, and their functions in widespread applications — A comprehensive review, Adv. Drug Deliv. Rev. 107 (2016) 367–392. https://doi.org/10.1016/j.addr.2016.06.012.
[8] S. Inkinen, M. Hakkarainen, A.-C. Albertsson, A. Södergård, From Lactic acid to Poly(lactic acid) (PLA): Characterization and analysis of PLA and its precursors, Biomacromolecules. 12 (2011) 523–532. https://doi.org/10.1021/bm101302t.
[9] J. Shao, S. Xiang, X. Bian, J. Sun, G. Li, X. Chen, Remarkable Melting Behavior of PLA Stereocomplex in Linear PLLA/PDLA Blends, Ind. Eng. Chem. Res. 54 (2015) 2246–2253. https://doi.org/10.1021/ie504484b.
[10] A. Tor-Świątek, T. Garbacz, V. Sedlarik, P. Stloukal, P. Kucharczyk, Influence of Polylactide modification with blowing agents on selected mechanical properties, Adv. Sci. Technol. Res. J. 11 (2017) 206–214. https://doi.org/10.12913/22998624/80850.
[11] J.-H. Seo, J. Han, K.S. Lee, S.W. Cha, Combined effect of chemical and microcellular foaming on foaming characteristics of PLA in injection molding, Polym.-Plast. Technol. Eng. 51 (2012) 455–460. https://doi.org/10.1080/03602559.2011.651239.
[12] J. Ludwiczak, M. Kozlowski, Dynamic Mechanical Properties of Foamed Polylactide and Polylactide/Wood Flour Composites, J. Biobased Mater. Bioenergy. 9 (2015) 227–230. https://doi.org/10.1166/jbmb.2015.1502.
[13] J. Ludwiczak, S. Frackowiak, R. Tuzny, Effect of recycling on the cellular structure of polylactide in a batch process, Cell. Polym. 37 (2018) 69–79. https://doi.org/10.1177/026248931803700202.
[14] J.A. Villamil Jiménez, N. Le Moigne, J.-C. Benezet, M. Sauceau, R. Sescousse, J. Fages, Foaming of PLA composites by supercritical fluid-assisted processes: A review, Molecules. 25 (2020) 3408. https://doi.org/doi:10.3390/molecules25153408.
[15] E. Di Maio, E. Kiran, Foaming of polymers with supercritical fluids and perspectives on the current knowledge gaps and challenges, J. Supercrit. Fluids. 134 (2018) 157–166. https://doi.org/10.1016/j.supflu.2017.11.013.
[16] S.P. Nalawade, F. Picchioni, L.P.B.M. Janssen, Supercritical carbon dioxide as a green solvent for processing polymer melts: Processing aspects and applications, Prog. Polym. Sci. 31 (2006) 19–43. https://doi.org/10.1016/j.progpolymsci.2005.08.002.
[17] S.K. Goel, E.J. Beckman, Generation of microcellular polymeric foams using supercritical carbon dioxide. II: Cell growth and skin formation, Polym. Eng. Sci. 34 (1994) 1148–1156. https://doi.org/10.1002/pen.760341408.
[18] S.K. Goel, E.J. Beckman, Nucleation and growth in microcellular materials: Supercritical supercooling as foaming agent, AIChE J. 41 (1995) 357–367. https://doi.org/10.1002/aic.690410217.
[19] S.K. Goel, E.J. Beckman, Generation of microcellular polymeric foams using supercritical carbon dioxide. I: Effect of pressure and temperature on nucleation, Polym. Eng. Sci. 34 (1994) 1137–1147. https://doi.org/10.1002/pen.760341407.
[20] J.E. Weller, V. Kumar, Solid-state microcellular polycarbonate foams. I. The steady-state process space using subcritical carbon dioxide, Polym. Eng. Sci. 50 (2010) 2160–2169. https://doi.org/10.1002/pen.21736.
[21] J.E. Weller, V. Kumar, Solid-state microcellular polycarbonate foams. II. The effect of cell size on tensile properties, Polym. Eng. Sci. 50 (2010) 2170–2175. https://doi.org/10.1002/pen.21737.

[22] M. Wessling, Z. Borneman, Th. Van Den Boomgaard, C.A. Smolders, Carbon dioxide foaming of glassy polymers, J. Appl. Polym. Sci. 53 (1994) 1497–1512. https://doi.org/10.1002/app.1994.070531112.
[23] V. Kumar, P.J. Stolarczuk, Microcellular PET foams produced by the solid state process, in: Imaging Image Anal. Appl. Plast., Elsevier, 1999: pp. 241–247. https://doi.org/10.1016/B978-188420781-5.50030-9.
[24] C. Fan, C. Wan, F. Gao, C. Huang, Z. Xi, Z. Xu, L. Zhao, Extrusion foaming of poly(ethylene terephthalate) with carbon dioxide based on rheology analysis, J. Cell. Plast. 52 (2016) 277–298. https://doi.org/10.1177/0021955X14566085.
[25] D. Li, T. Liu, L. Zhao, W. Yuan, Controlling sandwich-structure of PET microcellular foams using coupling of supercooling diffusion and induced crystallization, AIChE J. 58 (2012) 2512–2523. https://doi.org/10.1002/aic.12764.
[26] A. Arora, J. Lesser, J. McCarthy, Prepration and characterization of microcellular polystyrene foams processed in supercritical carbon dioxide, Macromolecules. 31 (1998) 4614–4620. https://doi.org/10.1021/ma971811z.
[27] J.S. Colton, N.P. Suh, The nucleation of microcellular thermoplastic foam with additives: Part I: Theoretical considerations, Polym. Eng. Sci. 27 (1987) 485–492. https://doi.org/10.1002/pen.760270702.
[28] C.M. Stafford, T.P. Russell, T.J. McCarthy, Expansion of polystyrene using supercritical carbon dioxide: effects of molecular weight, polydispersity, and low molecular weight components, Macromolecules. 32 (1999) 7610–7616. https://doi.org/10.1021/ma9902100.
[29] E. Reverchon, S. Cardea, Production of controlled polymeric foams by supercritical CO_2, J. Supercrit. Fluids. 40 (2007) 144–152. https://doi.org/10.1016/j.supflu.2006.04.013.
[30] P. Handa, B. Wong, Z. Zhang, V. Kumar, S. Eddy, K. Khemani, Some thermodynamic and kinetic properties of the system PETG-CO_2, and morphological characteristics of the CO_2-blown PETG foams, Polym. Eng. Sci. 39 (1999) 55–61. https://doi.org/10.1002/pen.11396.
[31] P. Handa, B. Wong, Z. Zhang, V. Kumar, S. Eddy, K. Khemani, CO_2 -Blown PETG Foams, in: Imaging Image Anal. Appl. Plast., Elsevier, 1999: pp. 165–171. https://doi.org/10.1016/B978-188420781-5.50021-8.
[32] C.A. Diaz, L.M. Matuana, Continuous extrusion production of microcellular rigid PVC, J. Vinyl Addit. Technol. 15 (2009) 211–218. https://doi.org/10.1002/vnl.20205.
[33] Z. Xu, X. Jiang, T. Liu, G. Hu, L. Zhao, Z. Zhu, W. Yuan, Foaming of polypropylene with supercritical carbon dioxide, J. Supercrit. Fluids. 41 (2007) 299–310. https://doi.org/10.1016/j.supflu.2006.09.007.
[34] B. Park, K. Cheung, A study of cell nucleation in the extrusion of polypropylene foams, Polym. Eng. Sci. 37 (1997) 1–10. https://doi.org/10.1002/pen.11639.
[35] Z. Yang, T. Liu, D. Hu, Z. Xu, L. Zhao, Foaming window for preparation of microcellular rigid polyurethanes using supercritical carbon dioxide as blowing agent, J. Supercrit. Fluids. 147 (2019) 254–262. https://doi.org/10.1016/j.supflu.2018.11.001.
[36] W. Zhai, W. Feng, J. Ling, W. Zheng, Fabrication of lightweight microcellular polyimide foams with three-dimensional shape by CO_2 foaming and compression molding, Ind. Eng. Chem. Res. 51 (2012) 12827–12834. https://doi.org/10.1021/ie3017658.
[37] S. Cotugno, E. Di Maio, G. Mensitieri, S. Iannace, G.W. Roberts, R.G. Carbonell, H.B. Hopfenberg, Characterization of microcellular biodegradable polymeric foams produced from supercritical carbon dioxide solutions, Ind. Eng. Chem. Res. 44 (2000) 1795–1803. https://doi.org/10.1021/ie049445c.
[38] A. Salerno, E. Di Maio, S. Iannace, P.A. Netti, Solid-state supercritical CO_2 foaming of PCL and PCL-HA nano-composite: Effect of composition, thermal history and foaming process on foam pore structure, J. Supercrit. Fluids. 58 (2011) 158–167. https://doi.org/10.1016/j.supflu.2011.05.009.
[39] H. Zhang, G.M. Rizvi, C.B. Park, Development of an extrusion system for producing fine-celled HDPE/wood-fiber composite foams using supercooling as a blowing agent, Adv. Polym. Technol. 23 (2004) 263–276. https://doi.org/10.1002/adv.20016.

[40] T. Kuang, H. Mi, D. Fu, X. Jing, B. Chen, W. Mou, X. Peng, Fabrication of Poly(lactic acid)/Graphene oxide foams with highly oriented and elongated cell structure via unidirectional foaming using supercritical carbon dioxide, Ind. Eng. Chem. Res. 54 (2015) 758–768. https://doi.org/10.1021/ie503434q.
[41] G. Gedler, M. Antunes, J. Velasco, Effects of graphene nanoplatelets on the morphology of polycarbonate–graphene composite foams prepared by supercritical carbon dioxide two-step foaming, J. Supercrit. Fluids. 100 (2015) 167–174. https://doi.org/10.1016/j.supflu.2015.02.005.
[42] Y.H. Lee, T. Kuboki, C.B. Park, M. Sain, The effects of nanoclay on the extrusion foaming of wood fiber/polyethylene nanocomposites, Polym. Eng. Sci. 51 (2011) 1014–1022. https://doi.org/10.1002/pen.21739.
[43] X. Han, C. Zeng, L.J. Lee, K.W. Koelling, D.L. Tomasko, Extrusion of polystyrene nanocomposite foams with supercritical supercooling, Polym. Eng. Sci. 43 (2003) 1261–1275. https://doi.org/10.1002/pen.10107.
[44] N. Le Moigne, M. Sauceau, M. Benyakhlef, J.-C. Jemai R. and Benezet, E. Rodier, J.-M. Lopez-Cuesta, J. Fages, Foaming of poly(3-hydroxybutyrate-co-3-hydroxyvalerate)/organo-clays nano-biocomposites by a continuous supercritical supercooling assisted extrusion process, Eur. Polym. J. 61 (2014) 157–171. https://doi.org/10.1016/j.eurpolymj.2014.10.008.
[45] N. Najafi, M.-C. Heuzey, P.J. Carreau, D. Therriault, C.B. Park, Rheological and foaming behavior of linear and branched polylactides, Rheol. Acta. 53 (2014) 779–790. https://doi.org/10.1007/s00397-014-0801-3.
[46] H. Zhou, M. Zhao, Z. Qu, J. Mi, X. Wang, Y. Deng, Thermal and Rheological Properties of Poly(lactic acid)/Low-Density Polyethylene Blends and Their Supercritical O_2 Foaming Behavior, J. Polym. Environ. 26 (2018) 3564–3573. https://doi.org/10.1007/s10924-018-1240-5.
[47] Y.-M. Corre, A. Maazouz, J.J. Duchet, Batch foaming of chain extended PLA with supercritical CO_2: Influence of the rheological properties and the process parameters on the cellular structure, J. Supercrit. Fluids. 58 (2011) 177–188. https://doi.org/10.1016/j.supflu.2011.03.006.
[48] E. Richards, R. Rizvi, A. Chow, H. Naguib, Biodegradable Composite Foams of PLA and PHBV Using Subcritical CO_2, J. Polym. Environ. 16 (2008) 258–266. https://doi.org/10.1007/s10924-008-0110-y.
[49] B. Mallet, K. Lamnawar, A. Maazouz, Compounding and melt strengthening of Poly(Lactic Acid): Shear and elongation rheological investigations for forming process, Key Eng. Mater. 554–557 (2013) 1751–1756. https://doi.org/10.4028/www.scientific.net/KEM.554-557.1751.
[50] S. Xue, P. Jia, Q. Ren, X. Liu, R.E. Lee, W. Zhai, Improved expansion ratio and heat resistance of microcellular poly(L-lactide) foam via in-situ formation of stereocomplex crystallites, J. Cell. Plast. 54 (2018) 103–119. https://doi.org/10.1177/0021955X16670587.
[51] L. Wei, H. Shicheng, Z. Hongfu, Effect of octa(epoxycyclohexyl) POSS on thermal, rheology property, and foaming behavior of PLA composites, J. Appl. Polym. Sci. 135 (2018) 46399. https://doi.org/10.1002/app.46399.
[52] L.-Q. Xu, H. Huang, Foaming of Poly(lactic acid) using supercritical carbon dioxide as foaming agent: Influence of crystallinity and spherulite size on cell structure and expansion ratio, Ind. Eng. Chem. Res. 53 (2014) 2277–2286. https://doi.org/10.1021/ie403594t.
[53] J. Wang, W. Zhu, H. Zhang, C.B. Park, Continuous processing of low-density, microcellular poly(lactic acid) foams with controlled cell morphology and crystallinity, Chem. Eng. Sci. 75 (2012) 390–399. https://doi.org/10.1016/j.ces.2012.02.051.
[54] J.-W. Chen, J.-L. Liu, Batch-foamed biodegradable polylactide acid/organic modified montmorillonite clays and polylactide/sericite powder nanocomposites, J. Polym. Eng. 32 (2012). https://doi.org/10.1515/polyeng-2011-0148.
[55] H. Zhao, G. Zhao, L.-S. Turng, X. Peng, Enhancing nanofiller dispersion through prefoaming and its effect on the microstructure of microcellular injection molded polylactic acid/clay

nanocomposites, Ind. Eng. Chem. Res. 54 (2015) 7122–7130. https://doi.org/10.1021/acs.iecr.5b01130.
[56] A. Kramschuster, L.-S. Turng, An injection molding process for manufacturing highly porous and interconnected biodegradable polymer matrices for use as tissue engineering scaffolds, J. Biomed. Mater. Res. B Appl. Biomater. 9999B (2009) 11. https://doi.org/10.1002/jbm.b.31523.
[57] M. Nofar, C.B. Park, Poly (lactic acid) foaming, Prog. Polym. Sci. 39 (2014) 1721–1741. https://doi.org/10.1016/j.progpolymsci.2014.04.001.
[58] M. Chauvet, M. Sauceau, F. Baillon, J. Fages, Mastering the structure of PLA foams made with extrusion assisted by supercritical CO_2, J. Appl. Polym. Sci. 134 (2017) 45067. https://doi.org/10.1002/app.45067.
[59] Å. Larsen, C. Neldin, Physical extruder foaming of poly(lactic acid)-processing and foam properties, Polym. Eng. Sci. 53 (2013) 941–949. https://doi.org/10.1002/pen.23341.
[60] M. Mihai, M.A. Huneault, B.D. Favis, H. Li, Extrusion foaming of semi-crystalline PLA and PLA/Thermoplastic starch blends, Macromol. Biosci. 7 (2007) 907–920. https://doi.org/10.1002/mabi.200700080.
[61] L.M. Matuana, C.A. Diaz, Study of cell nucleation in microcellular Poly(lactic acid) foamed with supercritical CO_2 through a continuous-extrusion process, Ind. Eng. Chem. Res. 49 (2010) 2186–2193. https://doi.org/10.1021/ie9011694.
[62] K. Bocz, T. Tabi, D. Vadas, M. Sauceau, J. Fages, Gy. Marosi, Characterisation of natural fibre reinforced PLA foams prepared by supercritical supercooling assisted extrusion, Express Polym. Lett. 10 (2016) 771–779. https://doi.org/10.3144/expresspolymlett.2016.71.
[63] K. Taki, D. Kitano, M. Ohshima, Effect of growing crystalline phase on bubble nucleation in Poly(Lactide)/CO_2 batch foaming, Ind. Eng. Chem. Res. 50 (2011) 3247–3252. https://doi.org/10.1021/ie101637f.
[64] J.R. Dorgan, J.S. Williams, D.N. Lewis, Melt rheology of poly(lactic acid): Entanglement and chain architecture effects, J. Rheol. 43 (1999) 1141–1155. https://doi.org/10.1122/1.551041.
[65] D. Carlson, P. Dubois, L. Nie, R. Narayan, Free radical branching of polylactide by reactive extrusion, Polym. Eng. Sci. 38 (1998) 311–321. https://doi.org/10.1002/pen.10192.
[66] S. Iannace, L. Nicolais, Isothermal crystallization and chain mobility of poly(L-lactide), J. Appl. Polym. Sci. 64 (1996) 911–919. https://doi.org/doi.org/10.1016/j.polymer.2020.122373.
[67] L.-T. Lim, R. Auras, M. Rubino, Processing technologies for poly(lactic acid), Prog. Polym. Sci. 33 (2008) 820–852. https://doi.org/10.1016/j.progpolymsci.2008.05.004.
[68] J.R. Dorgan, J. Janzen, M.P. Clayton, S.B. Hait, D.M. Knauss, Melt rheology of variable L content poly(lactic acid), J. Rheol. 49 (2005) 607–619. https://doi.org/10.1122/1.1896957.
[69] M. Righetti, P. Cinelli, N. Mallegni, C. Massa, S. Bronco, A. Stäbler, A. Lazzeri, Thermal, mechanical, and rheological properties of biocomposites made of Poly(lactic acid) and potato pulp powder, Int. J. Mol. Sci. 20 (2019) 675. https://doi.org/10.3390/ijms20030675.
[70] S. Faba, M.P. Arrieta, Á. Agüero, A. Torres, J. Romero, A. Rojas, M.J. Galotto, Processing Compostable PLA/Organoclay Bionanocomposite Foams by Supercritical CO2 Foaming for Sustainable Food Packaging, Polymers. 14 (2022) 4394. https://doi.org/10.3390/polym14204394.
[71] B. Li, G. Zhao, G. Wang, L. Zhang, J. Gong, Fabrication of high-expansion microcellular PLA foams based on pre-isothermal cold crystallization and supercritical CO_2 foaming, Polym. Degrad. Stab. 156 (2018) 75–88. https://doi.org/10.1016/j.polymdegradstab.2018.08.009.
[72] S. Pilla, S.G. Kim, G.K. Auer, S. Gong, C.B. Park, Microcellular extrusion foaming of poly(lactide)/poly(butylene adipate-co-terephthalate) blends, Mater. Sci. Eng. C. 30 (2010) 255–262. https://doi.org/10.1016/j.msec.2009.10.010.
[73] S. Pilla, S.G. Kim, G.K. Auer, S. Gong, C.B. Park, Microcellular extrusion-foaming of polylactide with chain-extender, Polym. Eng. Sci. 49 (2009) 1653–1660. https://doi.org/10.1002/pen.21385.

[74] M. Nofar, Effects of nano-/micro-sized additives and the corresponding induced crystallinity on the extrusion foaming behavior of PLA using supercritical CO_2, Mater. Des. 101 (2016) 24–34. https://doi.org/10.1016/j.matdes.2016.03.147.
[75] M. Nofar, A. Tabatabaei, C.B. Park, Effects of nano-/micro-sized additives on the crystallization behaviors of PLA and PLA/supercooling mixtures, Polymer. 54 (2013) 2382–2391. https://doi.org/10.1016/j.polymer.2013.02.049.
[76] Y. Wu, S. Zhang, S. Han, K. Yu, L. Wang, Regulating cell morphology of poly (lactic acid) foams from microcellular to nanocellular by crystal nucleating agent, Polym. Degrad. Stab. 204 (2022) 110117. https://doi.org/10.1016/j.polymdegradstab.2022.110117.
[77] G. Zhou, W. Liu, H. Yin, Y. Zhang, C. Huang, Effect of nano-sized zinc citrate on the supercritical carbon dioxide-assisted extrusion foaming behavior of poly(lactic acid), J. Appl. Polym. Sci. 140 (2023) e53561. https://doi.org/10.1002/app.53561.
[78] Y. Su, P. Huang, J. Sun, J. Chen, H. Zheng, H. Luo, Y. Chong, Y. Zhao, F. Wu, W. Zheng, Extruded polylactide bead foams using anhydrous supercritical CO_2 extrusion foaming, J. Appl. Polym. Sci. (2023) e54557. https://doi.org/10.1002/app.54557.
[79] K. Shi, G. Liu, H. Sun, B. Yang, Y. Weng, Effect of Biomass as Nucleating Agents on Crystallization Behavior of Polylactic Acid, Polymers. 14 (2022) 4305. https://doi.org/10.3390/polym14204305.
[80] A. Bourmaud, J. Beaugrand, D.U. Shah, V. Placet, C. Baley, Towards the design of high-performance plant fibre composites, Prog. Mater. Sci. 97 (2018) 347–408. https://doi.org/10.1016/j.pmatsci.2018.05.005.
[81] R. Siakeng, M. Jawaid, H. Ariffin, S.M. Sapuan, M. Asim, N. Saba, Natural fiber reinforced polylactic acid composites: A review, Polym. Compos. 40 (2019) 446–463. https://doi.org/10.1002/pc.24747.
[82] R. Krishnamoorti, K. Yurekli, Rheology of polymer layered silicate nanocomposites, Curr. Opin. Colloid Interface Sci. 6 (2001) 464–470. https://doi.org/10.1016/S1359-0294(01)00121-2.
[83] S. Sinha Ray, M. Okamoto, Polymer/layered silicate nanocomposites: a review from preparation to processing, Prog. Polym. Sci. 28 (2003) 1539–1641. https://doi.org/10.1016/j.progpolymsci.2003.08.002.
[84] S.C. Cifuentes, E. Frutos, R. Benavente, V. Lorenzo, J.L. González-Carrasco, Assessment of mechanical behavior of PLA composites reinforced with Mg micro-particles through depth-sensing indentations analysis, J. Mech. Behav. Biomed. Mater. 65 (2017) 781–790. https://doi.org/10.1016/j.jmbbm.2016.09.013.
[85] H. Kargarzadeh, M. Mariano, J. Huang, N. Lin, I. Ahmad, A. Dufresne, S. Thomas, Recent developments on nanocellulose reinforced polymer nanocomposites: A review, Polymer. 132 (2017) 368–393. https://doi.org/10.1016/j.polymer.2017.09.043.
[86] N. Hijazi, N. Le Moigne, E. Rodier, M. Sauceau, T. Vincent, J.-C. Benezet, J. Fages, Biocomposite films based on poly(lactic acid) and chitosan nanoparticles: Elaboration, microstructural and thermal characterization: poly(lactic acid)/chitosan nanoparticles biocomposite films, Polym. Eng. Sci. 59 (2019) E350–E360. https://doi.org/10.1002/pen.24983.
[87] C.B. Park, A.H. Behravesh, R.D. Venter, Low density microcellular foam processing in extrusion using CO_2, Polym. Eng. Sci. 38 (1998) 1812–1823. https://doi.org/10.1002/pen.10351.
[88] B. Gupta, N. Revagade, J. Hilborn, Poly(lactic acid) fiber: An overview, Prog. Polym. Sci. 32 (2007) 455–482. https://doi.org/10.1016/j.progpolymsci.2007.01.005.
[89] F. Signori, M.-B. Coltelli, S. Bronco, Thermal degradation of poly(lactic acid) (PLA) and poly(butylene adipate-co-terephthalate) (PBAT) and their blends upon melt processing, Polym. Degrad. Stab. 94 (2009) 74–82. https://doi.org/10.1016/j.polymdegradstab.2008.10.004.
[90] M. Mihai, M.A. Huneault, B.D. Favis, Crystallinity development in cellular poly(lactic acid) in the presence of supercritical carbon dioxide, J. Appl. Polym. Sci. 113 (2009) 2920–2932. https://doi.org/10.1002/app.30338.

[91] M. Keshtkar, M. Nofar, C.B. Park, P.J. Carreau, Extruded PLA/clay nanocomposite foams blown with supercritical supercooling, Polymer. 55 (2014) 4077–4090. https://doi.org/10.1016/j.polymer.2014.06.059.
[92] E. Naguib, C.B. Park, N. Reichelt, Fundamental foaming mechanisms governing the volume expansion of extruded polypropylene foams, J. Appl. Polym. Sci. 91 (2004) 2661–2668. https://doi.org/10.1002/app.13448.
[93] J.A. Villamil Jiménez, N. Le Moigne, M. Sauceau, R. Sescousse, F. Espitalier, J.-C. Bénézet, J. Fages, Crystallisation of PLA-cellulose fibre composites and related rheological behaviour upon solidification effects of fibre size and shape distribution and concentration regimes, (submitted to publication).
[94] A. Jalali, S. Shahbikian, M. Huneault, S. Elkoun, Effect of molecular weight on the shear-induced crystallization of poly(lactic acid), Polymer. 112 (2017) 393–401. https://doi.org/10.1016/j.polymer.2017.02.017.
[95] X. Qian, X. Zhou, B. Mu, Z. Li, Fiber alignment and property direction dependency of FRC extrudate, Cem. Concr. Res. 33 (2003) 1575–1581. https://doi.org/10.1016/S0008-8846(03)00108-X.
[96] T. Rokkonen, H. Peltola, D. Sandquist, Foamability and viscosity behavior of extrusion foamed PLA–pulp fiber biocomposites, J. Appl. Polym. Sci. 136 (2019) 48202. https://doi.org/10.1002/app.48202.

Declaration of Competing Interest

The authors declare that they have no known competing financial interests or personal relationships that could have appeared to influence the work reported in this paper.

Graphical abstract

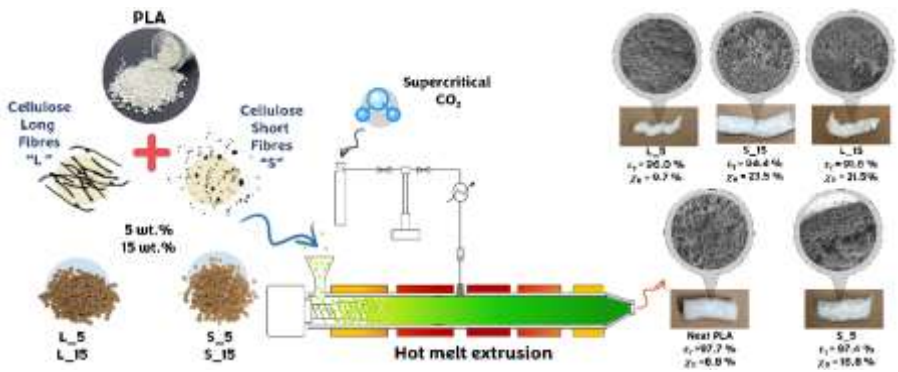

Highlights

- Foaming PLA-cellulose composites produce less expanded foams than neat PLA.
- Short fibres at low contents produce higher radially expanded foams than neat PLA.
- Long fibres at low contents increase longitudinal expansion of neat PLA foams.
- Degree of crystallinity of foams increases with fibre size and content.
- Foam structure is homogenised by increasing the fibre content.